Proceedings of CECNet 2022
A.J. Tallón-Ballesteros (Ed.)

doi:10.3233/FAIA220530

Quantitative Inversion Radar Imaging: A Physical Remote Sensing Modality of High Resolution

Shilong SUN [a,1], and Dahai DAI [a]
[a] *College of Electronic Science and Technology, National University of Defense Technology, Changsha, China*

Abstract. Quantitative inversion techniques have been widely used in many fields where the electric or magnetic fields are sampled in a wide range of viewing angles. In this paper, the quantitative inversion imaging scheme has been proposed for remote sensing radar systems with multiview-multistatic sensing configuration. The cross correlated contrast source inversion method is used in witch the cross-correlated term has been used as a regularization technique for, to some extent, overcoming the ill-posedness. Preliminary simulation results demonstrate that quantitative inversion radar imaging shows physical resolving ability for remote sensing imaging. To the best of our knowledge, it is verified for the first time that physical imaging is feasible with limited range of viewing angles (less than 65° in this paper). Therefore, we remark that in remote sensing applications, the quantitative inversion radar imaging scheme shows potential of identifying radar targets not only with finer geometric resolutions but also in an additional physical dimension of the electromagnetic characteristics. Extension of this inversion scheme to the multibistatic sensing configuration will be more impressive in the field of remote sensing radar imaging.

Keywords. Quantitative inversion, remote sensing, multiview-multistatic

1. Introduction

Electromagnetic (EM) inverse scattering is a procedure of recovering the morphological or EM characteristics using scattered fields detected at variant spatial locations. The forward and inverse scattering theory has important and extensive practical applications in many practical applications (such as geophysical survey [1], medical diagnosis [2,3], etc.). Inversion techniques have been investigated mainly in cases where the measurement data is obtained from a full aperture setup in order to circumvent the occurrence of local minima in the minimization process of the inversion.

In the classical radar signal processing theory, the point scattering center model is assumed, based upon which non-linear inverse scattering problems can be mathematically simplified with a linear model. Classical radar imaging theory has perfectly bal-

[1] Shilong Sun: College of Electronic Science and Technology, National University of Defense Technology, Changsha, China; E-mail: shilongsun@126.com.

anced the available computing resources at that time and forms the mature and unified radar language. Radar imaging methods based on matched filtering have been widely used in practical applications due to their efficient implementation algorithms and stable imaging performance, among which are the back-projection (BP) method [4], the Range-Doppler (RD) algorithm [5, Chapter 6], the range migration algorithm [6, Chapter 10], the time reversal (TR) technique [7], and so on. As is well known, the theoretical resolution of classical radar imaging is inevitably limited by the diffraction limit [8]. As a variant of the TR technique, the time-reversed multi-signal classification method (TR MUSIC) [9] enables finer resolution by exploiting the orthogonality of signal and noise. Compressive sensing technique also provides high imaging resolution by means of sparsity regularization with carefully selected trade-off parameters [10].

In contrast to the classical radar imaging theory, the EM inverse scattering theory depicts the EM scattering mechanism according to the EM wave equations and retrieve the EM characteristics of the scatterers by solving a nonlinear inverse problem. Inversion methods can be grouped into different categories from different perspectives, such as qualitative/quantitative inversion algorithms, local/global optimization algorithms, and so on. Among them, the inversion method based on the optimization of surface structure parameters [11,12] belongs to the qualitative inversion method. These methods require prior information about the location and number of the scatterers. The representative quantitative inversion methods include the contrast source inversion (CSI) method [13] and the Born/Distorted Born iterative methods (BIM and DBIM) [14], all of which belong to local optimization algorithms. Diffraction tomography (DT) [15,16] solves the nonlinear inverse scattering problem with Born approximation and the spatial spectrum of the contrast is achieved by processing the scattered field data probed by the receiving antennas in a certain way. In doing so, real-time inversion can be done with Fast Fourier transform (FFT). More importantly, the concept of the spatial spectrum provides clear insights into how the resolving ability of EM inversion is evaluated. The drawback of DT is the limit of weak targets, and we refer to a recent study [17] for reconstructing buried targets of high contrast with a modified DT method. In recent years, technologies such as artificial intelligence have also been applied in the field of EM inverse scattering [18,19,20], however relevant research is still in its infancy due to some fatal problems such as the poor generalization of neural networks.

As aforementioned, inversion imaging based on EM inverse scattering theory is mostly used in medical diagnosis and ground penetrating radar (GPR). In contrast to the classical radar imaging technology [5] which has been fully developed, the EM inversion technology based on the framework of EM inverse scattering theory has not been well applied in the radar systems of remote sensing such as air/space target imaging and etc., not to mention developing the inversion radar imaging systems. In this paper, we proposed the quantitative inversion imaging scheme for the radar obsvervation mode, and demonstrated (with preliminary simulation results) the better geometric and physical resolving ability in comparison to classical radar imaging. Quantitative inversion radar imaging is of physical resolving ability, because an quantitative inversion image consists of a permittivity image and a conductivity one, while in classical radar images only the relative magnitude of radar cross section (RCS) is given. Based on the above facts, we remark that the quantitative inversion radar imaging scheme can expand the dimension of information that can be obtained by remote sensing systems, and fundamentally improve the ability of radar systems in the aspect of target recognition.

The remainder of this paper is organized as follows: Section 2 gives the problem statement of radar imaging within the frameworks of classical radar imaging and EM inverse scattering theory, respectively; Section 3 introduces the inversion radar imaging scheme; Simulation experiments are presented in Section 4; Finally, Section 5 gives our conclusions.

2. Problem Statement

In general, radar imaging is a procedure of retrieving the 1-D, 2-D or even 3-D images of radar targets with the EM echo data. In this section, the problem statement of radar imaging is given within the frameworks of classical radar imaging and quantitative inversion radar imaging, respectively. The time factor $\exp(\mathrm{i}\omega t)$ is used and fixed for consistency in the remainder of this paper.

2.1. Electromagnetic Inverse Scattering Theory

2.1.1. Scattered field equation

The physical principle of the EM scattering in the framework of the inverse scattering theory is based on the EM wave equations, i.e., the Maxwell's equations. Mathematically, the inversion radar imaging is implemented by solving the parameters of Maxwell's equations. For 3-D EM inverse scattering problems, the scattered field equation can be obtained through the incident field equation and the total field equation, which can be formulated as follows

$$\nabla \times \boldsymbol{\mu}^{-1} \nabla \times \boldsymbol{E}_p^{\mathrm{sct}} - \omega^2 \boldsymbol{\varepsilon}_b \boldsymbol{E}_p^{sct} = \omega^2 \boldsymbol{\chi} \boldsymbol{E}_p^{\mathrm{tot}}, \tag{1}$$

where, the subscript p represents the field generated by the p-th source; the scattered field, $\boldsymbol{E}_p^{sct}$, is the difference of the total field and the incident field $\boldsymbol{E}_p^{\mathrm{sct}} = \boldsymbol{E}_p^{\mathrm{tot}} - \boldsymbol{E}_p^{\mathrm{inc}}$, $\boldsymbol{\mu}$ represents the permeability of the background media, which can be reasonably assumed as the permeability of free space, i.e., $\boldsymbol{\mu} = \boldsymbol{\mu}_0$; ω is the angular frequency; ε_{b} represents the complex permittivity in the form of $\boldsymbol{\varepsilon}_{\mathrm{b}} = \boldsymbol{\varepsilon}_{\mathrm{b}} - \mathrm{i}\boldsymbol{\sigma}_{\mathrm{b}}/\omega$, where, $\boldsymbol{\varepsilon}_{\mathrm{b}}$ is the background permittivity, $\boldsymbol{\sigma}_{\mathrm{b}}$ is the background conductivity, and $\boldsymbol{\chi}$ represents the difference of the complex permittivity of the scatterer and the background, which is referred to as the contrast. The formula of the contrast is given by $\boldsymbol{\chi} = (\boldsymbol{\varepsilon} - \boldsymbol{\varepsilon}_{\mathrm{b}}) - \mathrm{i}(\boldsymbol{\sigma} - \boldsymbol{\sigma}_{\mathrm{b}})/\omega$.

The scattered field, $\boldsymbol{E}_p^{sct}$, is equivalent with the echo signal data out of the frequency mixer in classical radar signal processing. In Cartesian coordinate system, if all parameters are assumed as constants in z-axis direction, the 3-D inverse scattering problem degrades to a 2-D one in x-y plane. If only z-polarized electric line sources are considered, we obtain the TM-polarized model of 2-D inverse scattering problems, for which only z-component of the electric field exists and the electric field is a scalar. Considering the stepped frequency signal as well, for a 2-D TM-polarized inversion radar imaging problem, the scattered field equation, Eq. (1), can be simplified as a scalar equation in the form of

$$-\nabla^2 E_{p,n}^{\mathrm{sct}} - k_n^2 E_{p,n}^{\mathrm{sct}} = \omega_n^2 \mu_0 J_{p,n} \tag{2}$$

where, ∇^2 is the Laplace operator, $p = 1, 2, \cdots, P$, $n = 0, 1, \cdots, N_f - 1$ represents different frequencies, $k_n = \omega_n \sqrt{\varepsilon_b \mu_0}$ is the wave number corresponding to the n-th frequency, J is referred to as the contrast source, which is the multiplication of the contrast and the total field. In the following of this paper, we shall firstly realize the inversion radar imaging with ideal TM-polarized synthetic data. The inversion radar imaging performance is quantitatively analyzed in comparison to the classical radar imaging.

3. Quantitative Inversion Radar Imaging

In inverse scattering problems, the inversion algorithms can be generally divided in the two families — local optimization algorithms and global optimization algorithms. In the remainder of this paper, a representative of local optimization algorithms — the cross-correlated contrast source inversion method (CC-CSI) — has been used to implement the quantitative inversion radar imaging scheme under the premise of zero prior information of the targets.

3.1. Formulation

In the EM inverse scattering theory, the measurement equation is referred to as data equation because it is in the data domain $\mathscr{S}$, and the data error equation is defined correspondingly as

$$\boldsymbol{\rho}_{p,n} = \boldsymbol{y}_{p,n} - \boldsymbol{\Phi}_{p,n} \omega_n^2 \boldsymbol{j}_{p,n}. \tag{3}$$

In addition, the state equation is defined in the state domain $\mathscr{D}$ by

$$\boldsymbol{e}_{p,n}^{\text{tot}} = \boldsymbol{e}_{p,n}^{\text{inc}} + \mathscr{M}_{\mathscr{D}} \boldsymbol{A}_n^{-1} \omega_n^2 \boldsymbol{\chi}_n \boldsymbol{e}_{p,n}^{\text{tot}}, \tag{4}$$

where, $\mathscr{M}_{\mathscr{D}}$ is the matrix for zeroing all values not in the inversion domain, $\boldsymbol{A}_n$ is the stiffness matrix in the finite difference frequency domain (FDFD) scheme. The state error equation is defined as

$$\boldsymbol{\gamma}_{p,n} = \boldsymbol{\chi}_n \boldsymbol{e}_{p,n}^{\text{inc}} - \boldsymbol{j}_{p,n} + \boldsymbol{\chi}_n \mathscr{M}_{\mathscr{D}} \boldsymbol{A}_n^{-1} \omega_n^2 \boldsymbol{\chi}_n \boldsymbol{e}_{p,n}^{\text{tot}}, \tag{5}$$

where, $\mathscr{M}_{\mathscr{D}}$ is a sampling matrix which constrains the state equation in the state domain. In the classical radar imaging, the data equation is linearized due to the assumption of the point scattering center model and then the solution is found which yields the relative values of the RCS distribution. Inversion radar imaging studied in this paper is based on the EM inverse scattering theory, and it solves the radar imaging problem not only with the data equation but also with the constraint of the state equation. This explains well why the former belongs to qualitative imaging, while the latter is able to do quantitative imaging. In the CC-CSI method, a new error referred to as the cross-correlated error is defined in the form of

$$\boldsymbol{\xi}_{p,n} = \boldsymbol{y}_{p,n} - \boldsymbol{\Phi}_{p,n} \left(\boldsymbol{\chi}_n \boldsymbol{e}_{p,n}^{\text{inc}} + \boldsymbol{\chi}_n \mathscr{M}_{\mathscr{D}} \boldsymbol{A}_n^{-1} \omega_n^2 \boldsymbol{\chi}_n \boldsymbol{e}_{p,n}^{\text{tot}} \right) \tag{6}$$

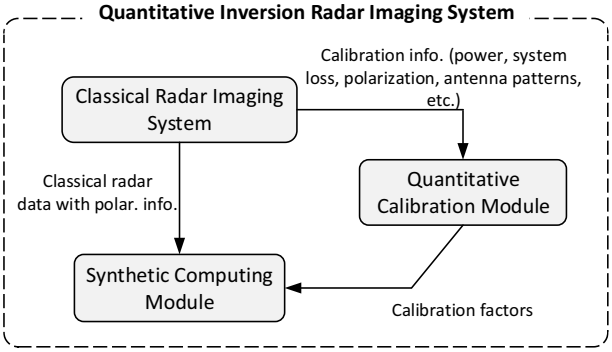

Figure 1. Basic diagram and data flow of a quantitative inversion radar imaging system.

The cross-correlated error is actually the mapping of the state error to the data domain. Both the state error and the cross-correlated error can be taken as constraints in solving the inverse scattering problem. Finally, the inversion radar imaging problem can be formulated as an optimization problem given by

$$\mathscr{C}_{\text{CC-CSI}}\left(\boldsymbol{\chi}_n, \boldsymbol{j}_{p,n}\right) = \sum_{n=0}^{N_f-1} \eta_n^{\mathscr{S}} \sum_{p=1}^{P} \left\| \boldsymbol{\rho}_{p,n} \right\|_{\mathscr{S}}^2 + \sum_{n=0}^{N_f-1} \eta_n^{D} \sum_{p=1}^{P} \left\| \boldsymbol{\gamma}_{p,n} \right\|_{D}^2 + \sum_{n=0}^{N_f-1} \eta_n^{\mathscr{S}} \sum_{p=1}^{P} \left\| \boldsymbol{\xi}_{p,n} \right\|_{\mathscr{S}}^2 \tag{7}$$

where,

$$\eta_n^{\mathscr{S}} = \left(\sum_{p=1}^{P} \left\| \boldsymbol{y}_{p,n} \right\|_{\mathscr{S}}^2 \right)^{-1}, \quad \eta_n^{\mathscr{D}} = \left(\sum_{p=1}^{P} \left\| \boldsymbol{\chi}_n \boldsymbol{e}_{p,n}^{\text{inc}} \right\|_{\mathscr{D}}^2 \right)^{-1} \tag{8}$$

are the weighting parameters in the data domain and the state domain, respectively; $\|\cdot\|_{\mathscr{S}}$ and $\|\cdot\|_{\mathscr{D}}$ represent the 2-norm in the data/state domains, respectively. CC-CSI is based on the gradient descent method in which the contrast source and the contrast are optimized sequentially in each iteration. We refer to [21,22] for more details of CC-CSI.

3.2. Incident Field Modeling

In the radar observation mode, the measurement data is generally the spatial samplings of the back-scattered fields. Since the TM-polarized 2-D radar imaging problem is considered in the following, the incident field modeling formula can be formulated as follows

$$E_{p,n}^{\text{inc}}\left(\boldsymbol{r}', \boldsymbol{r}_p, k_n\right) = \frac{1}{4}\omega_n \mu_0 H_0^{(1)}\left(-k_n \left\| \boldsymbol{r}' - \boldsymbol{r}_p \right\|\right). \tag{9}$$

Calibration is necessary to do exact inversion radar imaging. A complex factor is used to calibrate the incident field model, which is calculated using the back-scattered measurement data via the following equation

$$\alpha_{p,n} = \frac{y(\boldsymbol{r}, \boldsymbol{r}_p, k_n)}{E^{\text{inc}}_{p,n}(\boldsymbol{r}, \boldsymbol{r}_p, k_n)}. \tag{10}$$

Here we remark that a quantitative inversion radar imaging system must consist of a quantitative calibration module which gives real-time calibration factors for modeling the incident field and calibrating the probed data. Transmitting/receiving antenna patterns should be considered in the calibration module as well. Fig. 1 illustrates the diagram and data flow of a quantitative inversion radar imaging system, from which one can see that the design scheme of a quantitative inversion radar imaging system is an upgraded modality of the classical radar imaging system. Therefore, a quantitative inversion radar system is supposed to be of higher precision requirement than classical coherent imaging radar systems. In addition, thanks to the nonlinear scattering model, quantitative inversion radar imaging gives the fundamentally accurate understanding and interpretation of the HH, HV, VH and VV polarized data, instead of a direct addition process normally used in classical radar imaging.

4. Synthetic Data Inversion and Performance Analysis

In this section, we take the TM-polarized 2-D inverse scattering problem as an example for implementing the inversion radar imaging and analyzing its potential of physically classifying the target materials and the geometric resolutions in both range and azimuth directions. The synthetic data is processed by a classical radar imaging method — the BP imaging method — as well for comparison.

4.1. Simulation Experiment Parameters

The geometry of the 2-D simulation experiment is shown in Fig. 2. All the parameters involved are invariant in the z-axis direction. The red dots aligned in the line $y = 0$ represent the z-polarized electric line sources, the intervals of which are uniformly set to 0.1 m. And the blue ones in between represent the receiving antennas. If the number of the line sources is N, then there are $N+1$ receiving antennas in total. Stepped frequency signal is used. The initial frequency is $f_0 = 1$ GHz, the frequency step size is $\Delta f = 30$ MHz which gives an unambiguous range of 5 m. If the frequency number is N_f, then the bandwidth of the stepped frequency signal is $B = 30\left(N_f - 1\right)$. In the experiment, the multiple input multiple output (MIMO) measurement scheme is used, which means N times measurements are carried out and $(N+1) \times N_f$ complex data are sampled each time. Finally, we get a measurement data matrix $\boldsymbol{Y} \in \mathbb{C}^{N(N+1)\times N_f}$.

The synthetic data is generated by solving a 2-D forward scattering problem with an open source FDFD package [23] . Four perfectly matched layers (PMLs) are used at the boundary of the experiment region in the x-y plane and the two interfaces in the z-axis direction are set with periodic boundary condition (PBC). The spatial domain is discretized by $5 \times 5 \times 5$ mm^3 cubes ensuring that the ratio of the least wavelength ($f_{\max} = 2.35$ GHz) and the grid side length is greater than 25.

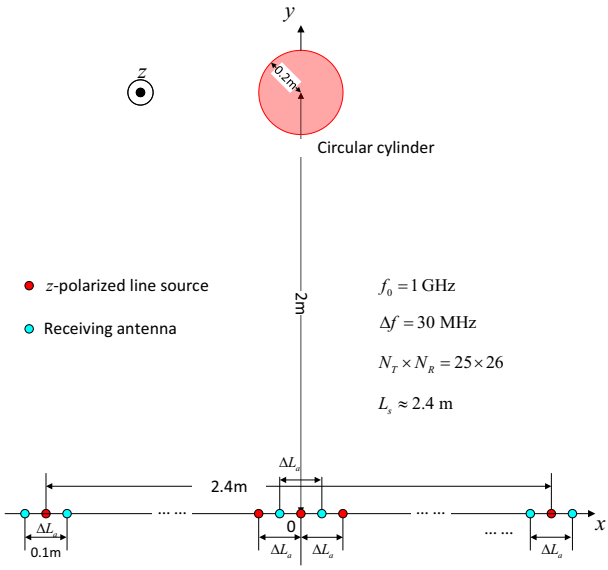

Figure 2. Geometry of the 2-D synthetic experiment scene with multiview-multistatic configuration.

4.2. Quantitative Imaging Results

Inversion radar imaging based on the EM inverse scattering theory belongs to quantitative imaging. Therefore, it is supposed to possess the potential of material classification based on the retrieved EM characteristics of the targets. In this subsection, we do inversion imaging to a combination of hybrid targets.

In this part, we do imaging to hybrid targets with noisy data. The targets consist of a square metallic cylinder of side length 0.3 m and a dielectric cylinder ($\varepsilon_r = 10$) of radius 0.15 m. The imaging parameters are $B = 1.35$ GHz and $L_a = 2.5$ m, which means we used 46 frequencies ranging from 1 GHz to 2.35 GHz and 24×25 transceivers. Complex Gaussian white noise is added to the synthetic data of the scattered E-field. Let us first process the synthetic data with SNR level of 10 dB, and Fig. 3(a) and (b,c) show the imaging results of the hybrid targets by BP and CC-CSI, respectively. From Fig. 3 we see that BP imaging successfully retrieves the boundary contour of the front side of the metallic square cylinder, however it fails to depict the arc contour of the dielectric circular one. The square cylinder shows slightly stronger RCS than the circular cylinder, but it exhibits no physical resolving ability. From Fig. 3(b) we see that the contour of the two cylinders has been successfully reconstructed. In Fig. 3(c), the square cylinder shows significantly higher conductivity (up to 200 mS/m) than the circular one, from which one can judge that the material of the square cylinder belongs to metal or highly lossy media. In the conductivity image of the circular cylinder, only a small fraction overlaps with its permittivity contrast image and the conductivity value is much less than the metallic one, indicating that the material of the circular cylinder belongs more likely to dielectric media of high contrast. Fig. 4 gives the imaging results by processing the noisy data of SNR $= 0$ dB, from which one can observe that quantitative inversion radar imaging is to some extend tolerant of noise. Simulation results show that, with the same sensing configuration and imaging parameters, the proposed quantitative inversion radar

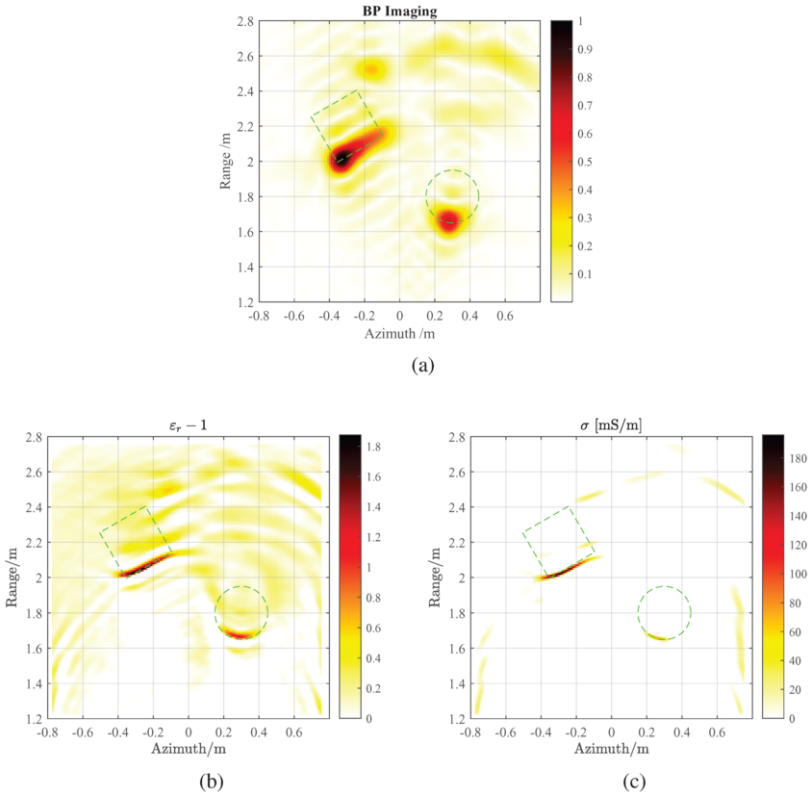

Figure 3. BP normalized amplitude image (a) and quantitative inversion images (contrast of permittivity (b) and conductivity (c)) of a metallic ($\sigma = \infty$) square cylinder of side length 0.3 m and a dielectric ($\varepsilon_r = 10$) circular cylinder of radius 0.15 m. Imaging parameters are $B = 1.35$ GHz and $L_a = 2.5$ m. SNR is 10 dB.

imaging scheme loses the physical resolving ability when SNR is less than -5 dB, and geometric resolving ability when SNR is less than -10 dB; while the lower SNR limit for BP imaging is -20 dB.

In the final, we remark that, on one hand, quantitative inversion radar imaging shows advantages over classical radar imaging with finer geometric resolutions, lower sidelobe levels and additional physical resolving ability; on the other hand, efforts are needed to overcome the following limitations

1. Although it exhibits good performance with a lower SNR, the robustness of quantitative inversion radar imaging against noise disturbance is not as good as classical radar imaging.
2. It is a tough task to do the incident field modling in real applications.
3. In this paper, the feasibility of the physical imaging has been demonstrated. However, methods need to be developed for multibistatic cases, which are widely involved in real applications.

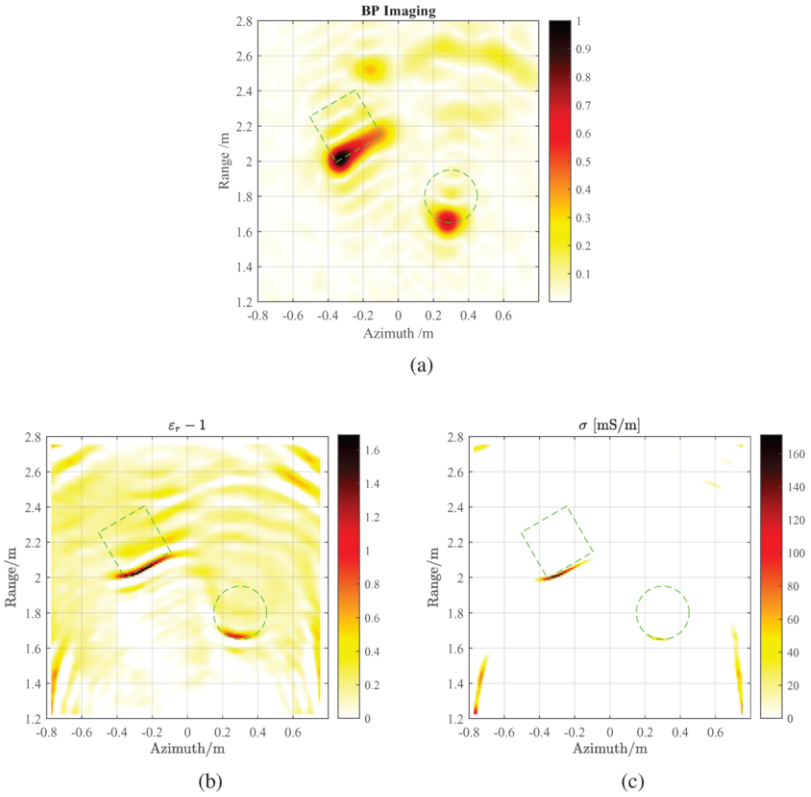

Figure 4. BP normalized amplitude image (a) and quantitative inversion images (contrast of permittivity (b) and conductivity (c)) of a metallic ($\sigma = \infty$) square cylinder of side length 0.3 m and a dielectric ($\varepsilon_r = 10$) circular cylinder of radius 0.15 m. Imaging parameters are $B = 1.35$ GHz and $L_a = 2.5$ m. SNR is 0 dB.

5. Conclusions

In this paper, the quantitative inversion imaging scheme has been proposed for the radar observation mode. Preliminary simulation results demonstrate that quantitative inversion radar imaging exhibits better (in comparison to classical radar imaging) and physical resolving ability, and it is to some extent tolerant of noisy data. Therefore, it is impressive to study the extension of quantitative imaging to multibistatic cases (such as Synthetic Aperture Radar (SAR) and Inverse SAR (ISAR)).

References

[1] S. Kuroda, M. Takeuchi, and H. J. Kim, "Full-waveform inversion algorithm for interpreting crosshole radar data: A theoretical approach," *Geosciences Journal*, vol. 11, no. 3, pp. 211–217, 2007.

[2] J. M. Rius, C. Pichot, L. Jofre, J.-C. Bolomey, N. Joachimowicz, A. Broquetas, and M. Ferrando, "Planar and cylindrical active microwave temperature imaging: numerical simulations," *IEEE transactions on medical imaging*, vol. 11, no. 4, pp. 457–469, 1992.

[3] C. Gilmore, A. Abubakar, W. Hu, T. M. Habashy, and P. M. Van Den Berg, "Microwave biomedical data inversion using the finite-difference contrast source inversion method," *IEEE Transactions on Antennas and Propagation*, vol. 57, no. 5, pp. 1528–1538, 2009.

[4] D. C. Munson, J. D. O'Brien, and W. K. Jenkins, "A tomographic formulation of spotlight-mode synthetic aperture radar," *Proceedings of the IEEE*, vol. 71, no. 8, pp. 917–925, 1983.
[5] I. G. Cumming and F. H. Wong, *Digital processing of synthetic aperture radar data*. Artech House Publishers, 2005.
[6] W. G. Carrara, R. S. Goodman, and R. M. Majewski, *Spotlight synthetic aperture radar: signal processing algorithms*. Norwood, MA: Artech House, 1995.
[7] M. Fink, "Time-reversal mirrors," *Journal of Physics D: Applied Physics*, vol. 26, no. 9, pp. 1333–1350, 1993.
[8] P. Zhang, X. Zhang, and G. Fang, "Comparison of the imaging resolutions of time reversal and back-projection algorithms in EM inverse scattering," *IEEE Geoscience and Remote Sensing Letters*, vol. 10, no. 2, pp. 357–361, 2013.
[9] A. Devaney, "Time reversal imaging of obscured targets from multistatic data," *IEEE Transactions on Antennas and Propagation*, vol. 53, no. 5, pp. 1600–1610, 2005.
[10] S. Sun, G. Zhu, and T. Jin, "Novel methods to accelerate CS radar imaging by NUFFT," *IEEE Transactions on Geoscience and Remote Sensing*, vol. 53, no. 1, pp. 557–566, 2015.
[11] T. Smith, M. Hoversten, E. Gasperikova, and F. Morrison, "Sharp boundary inversion of 2D magnetotelluric data," *Geophysical Prospecting*, vol. 47, no. 4, pp. 469–486, 1999.
[12] F. Santosa, "A level-set approach for inverse problems involving obstacles fadil santosa," *ESAIM: Control, Optimisation and Calculus of Variations*, vol. 1, pp. 17–33, 1996.
[13] P. M. Van Den Berg and R. E. Kleinman, "A contrast source inversion method," *Inverse problems*, vol. 13, no. 6, pp. 1607–1620, 1997.
[14] W. C. Chew and Y.-M. Wang, "Reconstruction of two-dimensional permittivity distribution using the distorted Born iterative method," *IEEE transactions on medical imaging*, vol. 9, no. 2, pp. 218–225, 1990.
[15] M. Slaney and A. C. Kak, "Imaging with diffraction tomography," Department of Electrical and Computer Engineering, Purdue University, West Lafayette, Indiana 47907, Tech. Rep. TR-EE 85-5, February 1985. [Online]. Available: https://docs.lib.purdue.edu/ecetr/540
[16] A. C. Kak and M. Slaney, *Principles of computerized tomographic imaging*. SIAM, 2001.
[17] M. Hajebi, A. Tavakoli, M. Dehmollaian, and P. Dehkhoda, "An iterative modified diffraction tomography method for reconstruction of a high-contrast buried object," *IEEE Transactions on Geoscience and Remote Sensing*, vol. 56, no. 7, pp. 4138–4148, 2018.
[18] E. Bermani, S. Caorsi, and M. Raffetto, "An inverse scattering approach based on a neural network technique for the detection of dielectric cylinders buried in a lossy half-space," *Progress In Electromagnetics Research*, vol. 26, pp. 67–87, 2000.
[19] ——, "Microwave detection and dielectric characterization of cylindrical objects from amplitude-only data by means of neural networks," *IEEE Transactions on Antennas and Propagation*, vol. 50, no. 9, pp. 1309–1314, 2002.
[20] L. Li, L. G. Wang, F. L. Teixeira, C. Liu, A. Nehorai, and T. J. Cui, "DeepNIS: Deep neural network for nonlinear electromagnetic inverse scattering," *IEEE Transactions on Antennas and Propagation*, vol. 67, no. 3, pp. 1819–1825, 2018.
[21] S. Sun, B. J. Kooij, T. Jin, and A. G. Yarovoy, "Cross-correlated contrast source inversion," *IEEE Transactions on Antennas and Propagation*, vol. 65, no. 5, pp. 2592–2603, 2017.
[22] S. Sun, B.-J. Kooij, and A. G. Yarovoy, "Inversion of multifrequency data with the cross-correlated contrast source inversion method," *Radio Science*, vol. 53, no. 6, pp. 710–723, 2018.
[23] W. Shin. (2015) MaxwellFDFD Webpage. https://github.com/wsshin/maxwellfdfd.